Received 11 October 2017; revised 7 February 2018; accepted 19 March 2018.
Date of publication 9 April 2018; date of current version 22 June 2018.

Digital Object Identifier 10.1109/JPETS.2018.2825142

Control of a PMSG Wind-Turbine Under Asymmetrical Voltage Sags Using Sliding Mode Approach

DEVBRATTA THAKUR (Student Member, IEEE), AND JIN JIANG (Fellow, IEEE)

Department of Electrical and Computer Engineering, University of Western Ontario, London, ON N6A 5B9, Canada
CORRESPONDING AUTHOR: J. JIANG (jjiang@eng.uwo.ca)

This work was supported by the Natural Sciences and Engineering Research Council of Canada.

ABSTRACT The control and operation of a grid-connected wind-turbine with a permanent magnet synchronous generator have been investigated under asymmetrical voltage sags at the grid side. To deal with such conditions, a fast-acting control scheme is needed. It is shown in this paper that a sliding mode control can meet the challenge. In the proposed control scheme, the dc link voltage, and active/reactive powers are decoupled first so that the asymmetrical voltage sag issues can be dealt with independently. To minimize additional stress inflicted by the asymmetrical voltage sag on the power electronic converters, a feed-forward negative sequence voltage is used in the vector current control strategy. Using the developed control scheme, the wind power generation system can remain on-line to support the grid even during the asymmetrical voltage sags. The effectiveness of the proposed control scheme has been validated by extensive simulations as well as through real-time hardware based experiments on a physical wind-turbine test platform.

INDEX TERMS Control of permanent magnet synchronous generator (PMSG), sliding mode control, voltage sag, wind turbine.

NOMENCLATURE

AC	Alternating current
AC	Alternating current
DC	Direct current
DGs	Distributed generators
DLV	DC link voltage
GSC	Grid side converter
LC	Inductor-capacitor filter
MPPT	Maximum power point tracking
MSC	Machine side converter
PCC	Point of common coupling
PCF	Power compensation factor
PI	Proportional-integral
PLL	Phase locked loop
PMSG	Permanent magnet synchronous generator
SMC	Sliding mode control
SRF	Synchronous reference frame
VCCF	Vector current control with feedforward
VSWT	Variable speed wind turbine
WES	Wind energy source.

I. INTRODUCTION

In recent years, small-scale wind-turbines combined with permanent magnet synchronous generators (PMSGs) are gaining popularity in distributed generation systems, due to their relatively small footprints, lower noise level, quick-payback, and capability to operate in either grid connected or islanded modes [1]. In a grid connected mode, these turbine-generator sets are often linked to a distribution network operating as active DGs. Being active DGs, they are also called up on to support the grid in an event of emergencies. One of such conditions is low voltage, such as asymmetrical voltage sags as defined in IEEE 1547 standard [2]. A wind-turbine-driven PMSG is a Type IV system, which is capable of performing grid support tasks because there is a full-scale frequency converter between the generator and the PCC [2]. Such converters can effectively isolate the generator from the grid so that desirable amount of active and reactive power can be injected into the grid independently.

As documented, an asymmetrical voltage sag can cause the following issues in a wind-turbine-driven PMSG system [3]: (1) double system frequency components would appear in the

injected currents due to the presence of negative sequence currents; (2) ripples with rising magnitude could occur in the DC link voltage due to unbalanced power flow between the generator and the grid side converter; and (3) the magnitude of the injected currents could rise beyond the safe operating limit of the inverter due to grid-side voltage sags. Furthermore, small-scale wind turbines are highly exposed to inherent transient disturbances such as frequent wind fluctuations, variations in loads, and intermittent faults. These disturbances undoubtedly create stress on the sensitive components in power electronic converters [4], where a large amplitude transient can cause catastrophic damage [5]. These issues, in fact, have limited the wide-spread adoption of small-scale grid-tied wind turbine systems. To increase the acceptance of such systems, impacts of asymmetrical grid voltage sags have to be reduced, so that the generator can remain connected to support the grid by injecting reactive power to improve the voltage profile at the PCC. However, a turbine-generator set is a highly non-linear system whose dynamic characteristics varies with the operating conditions and/or disturbances. This makes the design of a control system more challenging.

In the literature, there are some works on the control of power electronic converters (or inverters) and PMSG-based wind turbines. For example, different techniques for synthesis of current references under asymmetrical grid voltage profile have been studied in [6]. However, their impacts on the DC side under abnormal conditions have not been considered, neither did it try to limit the peak current in an event of voltage sags. The approaches taken in the literature, however, did not consider the grid disturbances [7]. A dual vector current controller is developed in [8], where two separate current controllers, one for positive and the other for negative synchronous reference frames, have been used. Unfortunately, this approach leads to a complex controller structure and potentially produces asymmetrical phase currents.

A current controller with positive-sequence grid voltage is used in the positive synchronous reference frame [9], but it does not completely address the issue of asymmetrical voltages. Controlling each phase separately by peak detection method (PDM) is also proposed for asymmetrical voltages [10], but such a strategy is hampered by PDM's sensitivity to low frequency fluctuations and harmonics.

A feed-forward power compensation technique has been investigated in [11] and [12]. In [11], sinusoidal balanced currents are obtained at the expense of DLV's oscillation and/or employment of a large DC link capacitor. Effective suppression of the increase in the grid current due to asymmetrical voltage sags has not been considered in [12]. This could lead to damage to power electronic components in the converter, unless overrated components are used. In addition, the control strategy requires real-time calculation of the compensating power, which is complex to implement and can add additional delay to the time required for the sequence extraction. Classical *PI* controllers are commonly used in the above-mentioned work. Such *PI* controllers perform well under small disturbances, but may not be able to cope with large ones, such as transients described in [13]. The non-linear characteristics of wind turbines require a controller that is sufficiently robust to the change in the dynamics due to variation of the operating conditions and/or in the presence of disturbances.

In this paper, a sliding mode vector current control scheme is developed, which is equipped with feed-forward of the negative sequence voltage to limit the injected current, eliminate the asymmetrical voltage sags, and suppress the impact of disturbances. The performance of the developed scheme has been validated by simulations and experiments under asymmetrical voltage sags at the PCC. The results have shown that the negative sequence current can be regulated to zero, a ripple-free DC link voltage has been maintained, the extracted frequency is free of any oscillations, and the output currents are maintained within the safe levels (pre-disturbed value). In addition, the dynamic behavior of the entire system has been improved over those with classical *PI* controllers. The robustness of SMC against parametric variations has also been improved. In summary, this paper has contributed to the safe and reliable operation of PMSG based wind turbine systems under asymmetrical voltage sags at the PCC, and makes it possible for ride through to support the grid during transients.

The paper is organized as follows. Section II describes the system under consideration and explains the problems to be addressed in this paper. The proposed SMC based control strategy is developed in Section III. The results of simulations and experimental investigation are presented in Section IV and V, respectively, and followed by conclusions in Sections VI.

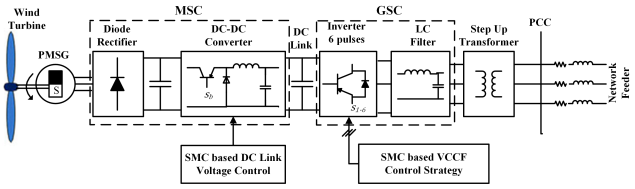

FIGURE 1. Schematic diagram of PMSG based variable speed wind turbine connected to a power grid network.

II. SYSTEM DESCRIPTION AND EXISTING PROBLEMS

A. SYSTEM DESCRIPTION

A wind turbine-driven PMSG investigated is shown in Fig.1. A two-stage power electronic converter is used to maintain system operation under the grid connected mode. The first stage consists of a three-phase diode rectifier plus a DC-DC converter (referred as MSC), and the second stage consists of an H-bridge of six pulse inverter (referred as GSC). The MSC is used to regulate the DLV in a voltage control mode with the inner current loop, whereas the GSC performs the power flow control based on a MPPT scheme. The LC filter is used in line with the inverter to provide a smooth and pure sinusoidal waveform, while the step-up transformer is used

to bring the inverter output voltage up to the grid level at the PCC. In this paper, the focus will be on the controller design and analysis for the above system under severe disturbances using a sliding mode VCCF of negative sequence currents to deal with asymmetrical grid voltage sags.

B. PROBLEMS TO BE INVESTIGATED AND CONTROL OBJECTIVES

In this paper, the focus will be on the controller design and analysis for the above system under severe disturbance conditions, such as asymmetrical grid voltage sags. An effective solution to the above problem is to use a VCCF of the negative sequence voltage, including the current limiting strategy using the sliding mode control approach. An SMC is insensitive to parameter changes and load disturbances, thus it is an effective control strategy for this situation [14].

Applications of SMC in wind turbines are not new. It has been shown that SMC can improve the performance over classical *PI* controllers under ideal grid conditions [15]. The effects of voltage sags can also be eliminated using a SMC approach [16]. However, asymmetrical conditions have not been considered therein. Similarly, the issues of rising the current amplitude due to voltage sags have not been considered [17] and [18]. Even though, a SMC based direct power control is implemented to achieve fast dynamics during asymmetrical voltage sags [17] and [18], however, the SMC control does not guarantee zero steady state error under all disturbances because no integral action is considered on the sliding surface. In addition, a high order compensator required to use the same sliding surface for multi-variables, which can be complicated to implement.

The number of differentiations of the output function required for the input to appear explicitly is known as the relative degree of the system [19]. The complexity in implementation of SMC arises with the relative degree of the system. The relative degree of the grid side converter is 2 as shown in [16]. In the developed control strategy, the dynamics associated with DLV, active power, and reactive power parts are decoupled. Hence, separate sliding surface is used for each variable resulting the relative degree being just one. The developed control strategy performs the following tasks:

(1) MSC - SMC based DC link voltage regulation; and

(2) GSC - SMC based VCCF for power control.

Thus, the SMC based VCCF and DLV regulation can eliminate oscillations in the injected current, reduce ripples and suppress the effects of disturbances. This allows the wind turbine to remain connected to the grid and to support the grid voltage with necessary reactive power. Further, the amplitude of the inverter current is also kept within the safe limits.

Two separate SMCs are used for DC-DC converter and inverter respectively. The SMC provides the control signal to the buck converter to maintain constant DLV, also for the inverter to maintain the output AC voltage with the desired injected grid current as shown in Fig.1. Therefore, the control objectives are to track the predefined inductor current and the output DC voltage for the DC-DC converter and $d-q$ axes currents. These $d-q$ axes currents are directly related to the active and reactive powers of the inverter.

III. PROPOSED SLIDING MODE CONTROL STRATEGY

The pre-defined sliding surface is chosen based on the desired behavior of the system as the states converge to this sliding surface. A general equation to represent the sliding surface is as follows [20]:

$$s = \left(\frac{d}{dt} + c\right)^{n-1} e \tag{1}$$

where c is a positive coefficient which is related to the bandwidth of the controller, e is the output error and n is the relative degree of the state variables. A Lyapunov approach is used to design the sliding surface for the control law that will drive the state along an equilibrium sliding surface. The Lyapunov function can be represented as follows:

$$W = \frac{s^T s}{2} > 0 \tag{2}$$

A necessary condition for the system to remain within the vicinity of the sliding surface or always converging to the sliding surface is $s\dot{s} < 0$. The switching function of the sliding mode controller ensures the stability by keeping the state trajectories on the sliding surface. Therefore, the switching control signal can be calculated based on the system behavior along the sliding manifold characterized as:

$$s = \dot{s} = 0 \tag{3}$$

A. MSC: DC LINK VOLTAGE REGULATION

A buck converter is used to regulate the output voltage or DLV (V_{dc}) for its simplicity. The dynamic model of the converter can be derived by using the generalized state space averaging method [21], which provides two sets of topological state-space equations as:

$$\begin{cases} \dfrac{di_{ind}}{dt} = \dfrac{1}{L_i}\left(d_c V_{in} - V_{dc}\right) \\ \dfrac{dV_{dc}}{dt} = \dfrac{1}{C_{dc}}\left(i_{ind} - \dfrac{V_{dc}}{R_l}\right) \end{cases} \tag{4}$$

where V_{in}, d_c, i_{ind}, L_i, C_{dc} and R_l are the input voltage, duty cycle of the pulse width modulation (PWM), inductor current, line inductor, DC link capacitor, and the load, respectively. The sliding surface for the output is chosen with a relative degree 1 from (1). The surface can be chosen as:

$$s = e \tag{5}$$

A linear combination of the state variables in (4) is set as the sliding surface of the converter:

$$e = ae_1 + be_2 + ce_3 = 0 \tag{6}$$

where a, b, and c are the coefficients of the SMC, while e_1, e_2, and e_3 are the current error, voltage error, and the integral

of these errors with different weights, which are defined as:

$$\begin{cases} e_1 = i_{ref} - i_{ind} \\ e_2 = V_{dcref} - V_{dc} \\ e_3 = \int (e_1 + ke_2)dt \end{cases} \quad (7)$$

where $i_{ref} = ke_2$ is the reference average inductor current, $k = \frac{1}{k_1}$, k_1 is the gain for the voltage error, and V_{dcref} is the reference DLV. Substituting (7) in (6) and using (5), the sliding surface becomes:

$$s = a\left(i_{ref} - i_{ind}\right) + b\left(V_{dcref} - V_{dc}\right) + c\int (e_1 + ke_2)dt = 0$$

Then, substituting i_{ref} and differentiating this equation with respect to time on both sides yields

$$\frac{ds}{dt} = ak\frac{dV_{dcref}}{dt} - ak\frac{dV_{dc}}{dt} - a\frac{di_{ind}}{dt} + b\frac{dV_{dcref}}{dt} - b\frac{dV_{dc}}{dt} + c\left(k+1\right)\left(V_{dcref} - V_{dc}\right) - ci_{ind} = 0 \quad (8)$$

Substituting (4) in (8) and replacing d_c by u_{eq}, the following is in order

$$\frac{ds}{dt} = -\frac{au_{eq}V_{in}}{L_i} + \frac{aV_{dc}}{L_i} - \frac{bi_{ind}}{C_{dc}} + \frac{bV_{dc}}{R_lC_{dc}} - \frac{aki_{ind}}{C_{dc}} + \frac{akV_{dc}}{R_lC_{dc}} + c\left(k+1\right)\left(V_{dcref} - V_{dc}\right) - ci_{ind} = 0 \quad (9)$$

From (9), u_{eq} can be derived as

$$u_{eq} = \frac{aR_lC_{dc}V_{dc} - \left(R_li_{ind} - V_{dc}\right)\left(bL_i + aL_ik\right)}{aR_lC_{dc}V_{in}} + \frac{cR_lL_iC_{dc}[2k\left(V_{dcref} - V_{dc}\right) - i_{ind}]}{aR_lC_{dc}V_{in}} \quad (10)$$

where u_{eq} is the equivalent control signal. The control law now becomes:

$$u_{st} = \begin{cases} 1 = ON, & if\ s > 0 \\ 0 = OFF, & if\ s \le 0 \end{cases} \quad (11)$$

This switching control ensures that the state trajectory is directed towards the sliding surface. However, it does not guarantee that the trajectory is maintained on the surface. Therefore, the condition as prescribed in terms of Lyapunov function in (2) must be satisfied to ensure that the trajectory is on the selected sliding surface. A combined switching function ($sf\ (t)$) ensures that the trajectory stays on the sliding surface.

$$sf\ (t) = u_{eq} + u_{st} \quad (12)$$

In this current work, (12) is used to implement the controller for regulating the DLV in the SMC scheme.

B. GSC: POWER INJECTION STRATEGY

The power reference is determined by the MPPT scheme to inject maximum power under normal conditions. However, the power production has to be reduced during an asymmetrical voltage sag for two reasons: (1) to balance the power flow with respect to the positive sequence voltage; and (2) to limit the current within the safe limit. The active power P and reactive power Q in d- q positive synchronous reference frame (SRF) can be represented as:

$$\begin{cases} P = \frac{3}{2}\left[V_{pdp}i_{pdp} + V_{pqp}i_{pqp}\right] \\ Q = \frac{3}{2}\left[-V_{pdp}i_{pqp} + V_{pqp}i_{pdp}\right] \end{cases} \quad (13)$$

where V_{pxx} and i_{pxx} are the primary side voltage and current, with subscripts d, q, p and n denoting d-axis, q-axis, positive sequence and negative sequence, respectively. The PLL regulates the positive sequence q-axis voltage to zero ($V_{pqp} = 0$) to extract the system frequency for synchronization. Therefore, the current references in d- q frame (i_{pdpref} and i_{pqpref}) can be calculated based on (13) as

$$\begin{cases} i_{pdpref} = \frac{2}{3V_{pdp}}P_{ref} \\ i_{pqpref} = -\frac{2}{3V_{pdp}}Q_{ref} \end{cases} \quad (14)$$

The reactive power reference Q_{ref} (i.e. the q-axis current reference, i_{pqpref}) is determined based on the appropriate grid code. Whereas the active power reference is derived from the apparent power and Q_{ref}.

From (14), the active power reference is obtained as

$$P_{ref} = 1.5V_{pdp}i_{pdpref} \quad (15)$$

When the grid voltage is symmetrical, the voltage is equal to the nominal rated voltage denoted by 'V_{nom}'. The power injected into the grid is equal to the maximum power (P_{mppt}) determined by the MPPT scheme, such that

$$P_{mppt} = 1.5V_{nom}i_{pdpref} \quad (16)$$

From (15) and (16), the reference power can be chosen as:

$$\begin{cases} P_{ref} = \frac{V_{pdp}}{V_{nom}}P_{mppt} \\ \text{PCF} = \frac{V_{pdp}}{V_{nom}} \end{cases} \quad (17)$$

The ratio between the positive sequence voltage and the nominal voltage is defined as the power compensation factor (PCF). As indicated in (17), the injected power during an asymmetrical voltage sag event will be proportional to the positive sequence voltage. For a given PCF, the reactive power demand is determined by the grid code. The active power flow can then be calculated using the apparent power from the MPPT algorithm and the demanded reactive power. In this way, the output current will be maintained within the rated limit of the inverter irrespective of the grid voltage conditions.

C. GSC: REGULATION OF THE NEGATIVE SEQUENCE CURRENT

The VCCF of the negative sequence voltage is proposed to cancel out the flow of the negative sequence currents during an asymmetrical grid voltage sag. Therefore, this control strategy requires information on the positive and the negative

sequences of the voltage, and the system frequency which can be extracted through a PLL as shown in Fig. 2.

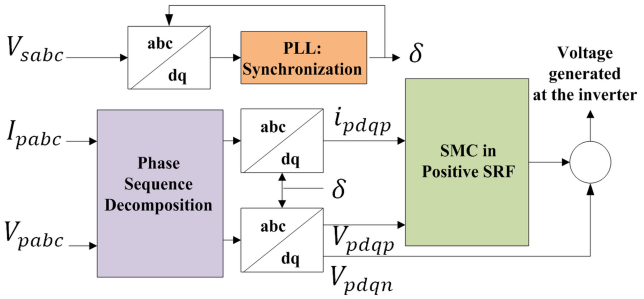

FIGURE 2. Control block diagram for VCCF.

In Fig. 2, parameters δ, V_{sxxx}, V_{pxxx}, and i_{pxxx} are the phase angle, secondary side voltage, primary side voltage, and primary side current, respectively, with subscripts abc, d, q, p and n denoting abc axes, $d-$axis, $q-$axis, positive sequence and negative sequence, respectively. The voltages and currents are decomposed into positive and negative sequence components, and then they are transformed into positive sequence $d-q$ coordinates as shown in Fig. 2. The vector current control using SMC is implemented in the positive SRF, while the negative sequence grid voltage is augmented with the current compensator output as a feed-forward term shown in Fig. 2. Therefore, the voltage generated at the inverter has the identical negative sequence voltage as in the grid voltage. Hence, the negative sequence voltage difference between the inverter terminal and the local grid will be zero. This means that the negative sequence current has been eliminated. Hence, only the positive sequence current flows into the grid.

The SMC is designed to generate the inverter output voltage, which is then used to produce PWM control signal. Hence, the output states are the primary side currents, i_{pdp} and i_{pqp}, in the positive sequence $d-q$ axis. These currents are then used to control the active and reactive power independently. The sliding surface is chosen with a relative degree 1 from (1).

One surface that satisfies the chosen output states can be chosen as:

$$s_1 = e_1 \quad \text{and } s_2 = e_2 \tag{18}$$

where $e_1 = i_{pdp} - i_{pdpref}$ and $e_2 = i_{pqp} - i_{pqpref}$.

The reference $d-$axis current i_{pdpref} is determined from the MPPT scheme to control the flow of the active power, whereas the reference $q-$axis current i_{pqpref} is obtained from the unity power factor operation or the voltage support mode to control the reactive power flow.

The sliding surfaces $s_1 = e_1 = 0$ and $s_2 = e_2 = 0$ indicate that the sliding mode occurs only at the origin. Therefore, smooth transients and robustness cannot be guaranteed in the transient state for all disturbances. To deal with this issue, an integral function is included in the sliding surface:

$$s_1 = e_1 + k_1 \int e_1 dt \tag{19}$$

$$s_2 = e_2 + k_2 \int e_2 dt \tag{20}$$

where k_1 and k_2 are integrator gains.

From (3), (19) and (20), one can have:

$$s_1 = s_2 = \dot{s}_1 = \dot{s}_2 = 0$$

$$\dot{s}_1 = \frac{de_1}{dt} + k_1 e_1 = 0 \tag{21}$$

$$\dot{s}_2 = \frac{de_2}{dt} + k_2 e_2 = 0 \tag{22}$$

Substitute e_1 in (21) by the error in current,

$$\dot{s}_1 = \frac{d(i_{pdp} - i_{pdpref})}{dt} + k_1(i_{pdp} - i_{pdpref}) = 0$$

$$or\ \dot{s}_1 = \frac{di_{pdp}}{dt} + k_1(i_{pdp} - i_{pdpref}) = 0 \tag{23}$$

The d- q components of the inverter AC side terminal voltage in positive sequence can then be represented as [22]

$$V_{pdp} = -L\left(\frac{di_{pdp}}{dt}\right) - Ri_{pdp} + \omega Li_{pqp} + V_{idp} \tag{24}$$

$$V_{pqp} = -L\left(\frac{di_{pqp}}{dt}\right) - Ri_{pqp} - \omega Li_{pdp} + V_{iqp} \tag{25}$$

where V_{idp}, V_{iqp}, R, and L are the positive sequence inverter output voltages in d- q axes, the line resistance, and the inductance of the LC filter at the output of the inverter.

Re-arranging (24) and substituting it into (23), it follows that

$$\dot{s}_1 = \frac{1}{L}(-V_{pdp} - Ri_{pdp} + \omega Li_{pqp} + V_{idp}) + k_1(i_{pdp} - i_{pdpref}) = 0$$

Define the following variables

$$f_1 = \frac{1}{L}\left(-V_{pdp} - Ri_{pdp} + \omega Li_{pqp}\right), \quad g_1 = \frac{1}{L},\ u_1 = V_{idp}$$

Then,

$$\dot{s}_1 = f_1 + g_1 u_1 \tag{26}$$

Similarly, (22) can be represented in the following form:

$$\dot{s}_2 = f_2 + g_2 u_2 \tag{27}$$

where

$$f_2 = \frac{1}{L}\left(-V_{pqp} - Ri_{pqp} - \omega Li_{pdp}\right), \quad g_2 = \frac{1}{L},\ u_2 = V_{iqp}$$

Using the following compact vector/matrix format

$$F = \begin{bmatrix} f_1 \\ f_2 \end{bmatrix}, \quad G = \begin{bmatrix} g_2 0 \\ 0 g_2 \end{bmatrix}, \quad U = \begin{bmatrix} V_{pdp} \\ V_{pqp} \end{bmatrix} \text{ and } s = \begin{bmatrix} s_1 \\ s_2 \end{bmatrix}$$

Taking the derivative of the Lyapunov function in (2) with respect to time, it follows:

$$\frac{dW}{dt} = s^T \frac{ds}{dt} \tag{28}$$

Substitute (26) and (27) in (28),

$$\frac{dW}{dt} = s^T (F + GU) \tag{29}$$

The switch control law can be chosen such that (29) is negative definite with $s \neq 0$, to guarantee the stability. Therefore, the control law can be chosen as

$$U = -G^{-1} \left\{ \begin{bmatrix} f_1 \\ f_2 \end{bmatrix} + \begin{bmatrix} -c_1 0 \\ 0 - c_2 \end{bmatrix} \begin{bmatrix} \tanh(s_1) \\ \tanh(s_2) \end{bmatrix} \right\} \tag{30}$$

where c_1 and c_2 are positive constants. The sliding surface dynamics are the tangent function of the surface such that the switching function is continuous and chatter free [23]. A block diagram of the proposed control scheme is shown in Fig. 3.

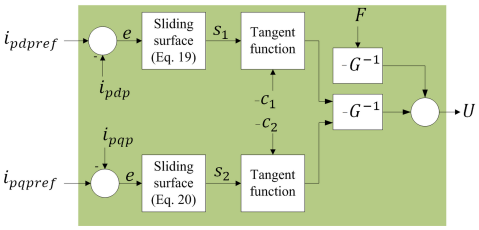

FIGURE 3. Developed SMC for inverter voltage output.

D. GSC: OVERALL CONTROL STRATEGY

The overall control strategy for the GSC is shown in Fig. 4.

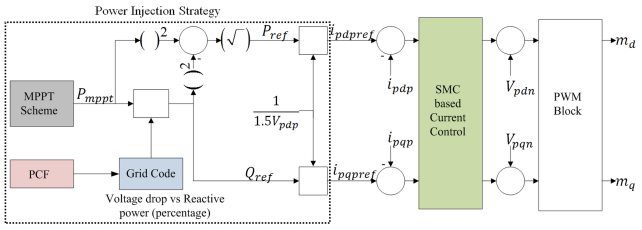

FIGURE 4. The overall control strategy for GSC in the positive sequence SRF.

This system can be categorized into three sections:

(1) *Power injection strategy:* The reference power is determined based on the grid code during a voltage disturbance at the PCC. The power indicated from the MPPT scheme is the apparent power. The control strategy in Fig. 4 can fulfill the reactive power requirements based on the grid code requirements. The active power is then determined based on the apparent power and the injected reactive power through PCF. The PCF carries the information about the voltage sag. If the grid is operating normally, the PCF would be unity. In this case, the WES is operating at the unity power factor under MPPT scheme. If the PCF < 1, the WES will inject adequate amount of active and reactive powers per grid requirements.

(2) *SMC based current control:* The negative sequence current is regulated to zero and the positive sequence current is allowed to flow from GSC to the PCC. This is accomplished by the control system as shown in Fig. 3.

(3) *PWM signal generation:* The sliding mode current controller is designed to regulate the inverter output voltage. The inputs are the SMC output signal and the feed-forward term of the negative sequence voltage. The modulating signals (m_d and m_q) at the outputs of the PWM can be expressed as:

$$\begin{cases} V_{idp} + V_{pdn} = \dfrac{V_{dc}}{2} m_d \\ V_{iqp} + V_{pqn} = \dfrac{V_{dc}}{2} m_q \end{cases} \tag{31}$$

The GSC terminal voltage in the positive sequence $d-q$ axis (V_{idp} and V_{iqp}), along with the negative sequence voltages as feed-forward terms and the DC link voltage, determine the modulating (control) signals. Since the flow of the negative sequence current is regulated to zero, only the positive sequence currents have to be considered in the control scheme.

IV. PERFORMANCE EVALUATION BY SIMULATION

The parameters of the wind turbine system and the grid used in this study are given in Appendix A. A grid disturbance causing an asymmetrical voltage sag is considered to validate the effectiveness of the developed control strategy. Transient disturbances, such as changes in wind speed and grid frequency, have also been considered. Properly designed *PI* controllers are used as a benchmark. They are designed using frequency response techniques to provide at least 60° phase margin.

A. CASE STUDY I: VARIATIONS IN WIND SPEED

The wind speed (normalized at 9.5 m/s) with turbulence effect is shown in Fig. 5 (a). The average wind speed is increased from 6.5m/s to 9m/s at 0.59s and then decreased to 6.5m/s at 1.01s. The reason for such a wind profile is to evaluate the performance of the control system in transient conditions.

The control signals for both *PI* and SMC are shown in Fig. 5 (b). As can be seen, the signal from the *PI* controller is more sluggish than that generated by the SMC. The *PI* controller tries to strike a balance between the overshoot and the settling time in the event of a disturbance. As such, the *PI* controller could not provide as effective stabilizing control as the SMC. As a result, the DLV undergoes both undershoot and overshoot of 9.2 % as shown in Fig. 5 (c). However, neither undershoots nor overshoots have been observed in the DLV with SMC. With the increased wind speed, the output power from the WES also increases. This is reflected in the increase of the output current when the grid voltage is kept constant. It is important to point out also that oscillatory responses in the current have been observed as shown in Fig. 5 (d) with *PI* controller.

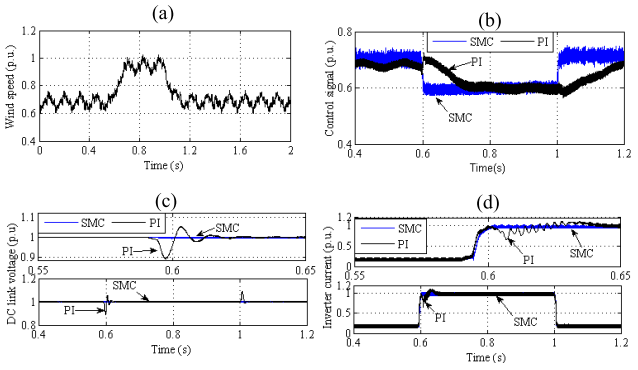

FIGURE 5. (a) Wind speed (normalized at 9.5 m/s), (b) Control signal, (c) DC link voltage (zoomed at upper display) and (d) Inverter current (zoomed at upper display).

However, no such oscillation exists when the SMC is used.

B. CASE STUDY II: VARYING SYSTEM FREQUENCY

To investigate the robustness of the developed SMC to the grid frequency variation, the grid frequency is deliberately reduced by a factor of 10 % (339.3 rad/s) at 0.591s and brought back to the nominal value (377 rad/s) at 0.91s as shown in Fig. 6 (a).

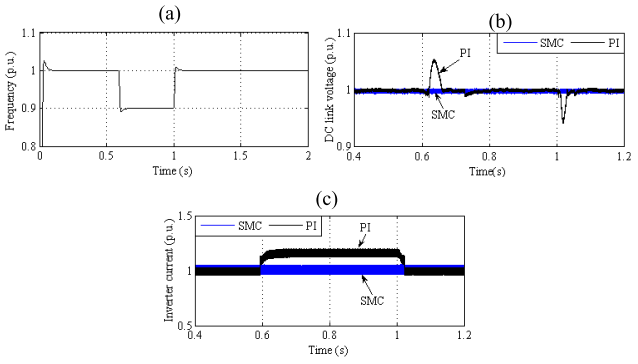

FIGURE 6. (a) System frequency-omega (rad/s), (b) DC link voltage (c) Inverter current.

Both overshoot and undershoot in DLV have been observed at 0.591s and 0.910s as shown in Fig. 6 (b) when the *PI* controller is used, but the system with the SMC is almost immune to the frequency disturbance. Similarly, the inverter output current is also maintained at the reference level under the SMC as shown in Fig. 6 (c). However, the current increases to the saturation level to compensate the frequency drop when the *PI* controller is used.

C. CASE STUDY III: ASYMMETRICAL GRID VOLTAGE SAG (87%, 37% AND 50 % DROP) WITH NO CONTROL

It is assumed that an asymmetrical grid voltage sag has occurred due to a sudden change in unbalanced loads. The asymmetrical loads considered are for 82 cycles starting at 0.174 s as shown in Fig. 7 (a). As a result, the negative sequence current appears as shown in Fig. 7 (b). Consequently, the inverter d- q axis positive sequence voltages and currents start to oscillate at twice of the system frequency as indicated in Fig. 7 (c) and (d). The voltage and current continue to oscillate for a few more cycles even after the clearance of the asymmetrical condition when the *PI* controller is used. In fact, the current hits the upper saturation limit for the pre-disturbed power reference and reduced voltages as shown in Fig. 7 (d). The DLV also oscillates at 20% in amplitude as shown in Fig. 7 (e). The rise in the DLV with oscillation indicates that the power flow is unbalanced between the generator and the GSC in the presence of negative sequence currents. The asymmetrical network voltage sag also destabilizes the system frequency as shown in Fig. 7 (f). The frequency (rad/s) is oscillating at (+/−) 15% around the nominal value.

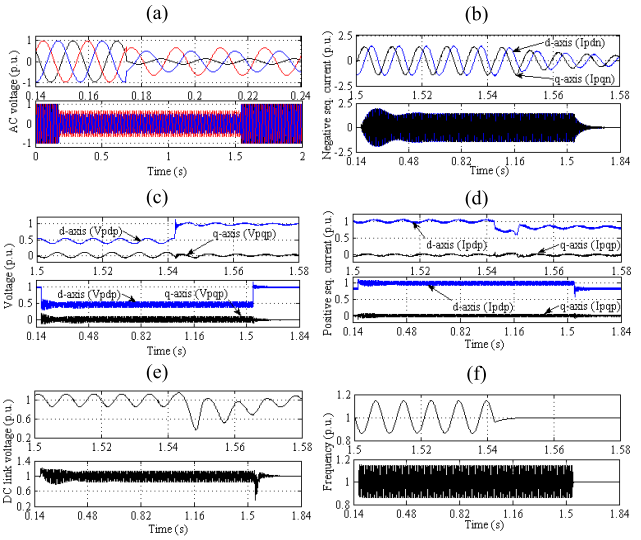

FIGURE 7. Wind system during an asymmetrical voltage sag with an PI control but without the proposed control strategy (zoomed version at upper display): (a) AC voltage at PCC, (b) Inverter negative sequence *d*- *q* axis currents (c) Inverter positive sequence *d*- *q* axis voltages (zoomed at upper display), (d) Inverter positive sequence *d*- *q* axis currents (zoomed at upper display), (e) DC link voltage (zoomed at upper display), and (f) Extracted per unit frequency-omega (rad/s) (zoomed at upper display).

D. CASE STUDY IV: ASYMMETRICAL GRID VOLTAGE SAG (87%, 37% AND 50 % DROP) WITH CONTROL

The wind system is operating as in *Case study III* but using the proposed control strategy as shown in Fig. 8. The negative sequence currents are regulated to zero as shown in Fig. 8 (b). Thus, there are no oscillations in the positive sequence voltages. However, the voltage sag still exists as shown in Fig. 8 (c). The $q-$axis voltage is regulated to zero by using the extracted system frequency from the PLL. The positive sequence $d-q$ axis currents are regulated per the grid code during the voltage sag as shown in Fig. 8 (d). The positive sequence $d-$axis current is reduced whereas the positive sequence q-axis current is increased to provide

the reactive power. The DLV is maintained at its reference level without any oscillation throughout this study as shown in Fig. 8 (e). The frequency has also been maintained at its nominal value (377 rad/s), as shown in Fig. 8 (f). Hence, it can be concluded that the developed SMC can provide much improved control over the *PI* controller under different grid and load conditions.

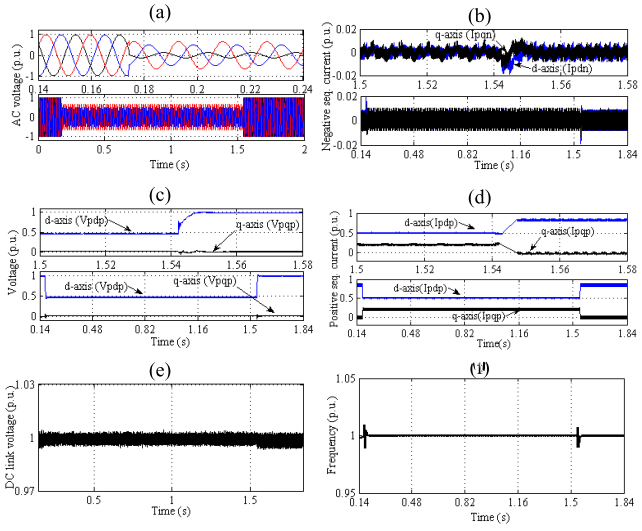

FIGURE 8. Wind system during an asymmetrical voltage sag with proposed SMC control (zoomed version at upper display): (a) AC voltage at PCC (b) Inverter negative sequence *d*- *q* axis currents, (c) Inverter positive sequence *d*- *q* axis voltages (zoomed at upper display), (d) Inverter positive sequence *d*- *q* axis currents (zoomed at upper display), (e) DC link voltage, and (f) Extracted per unit frequency-omega (rad/s).

V. EXPERIMENTAL VALIDATION

The effectiveness of the SMC based control strategy has also been validated on a lab-scale wind-turbine test facility as shown in Fig. 9.

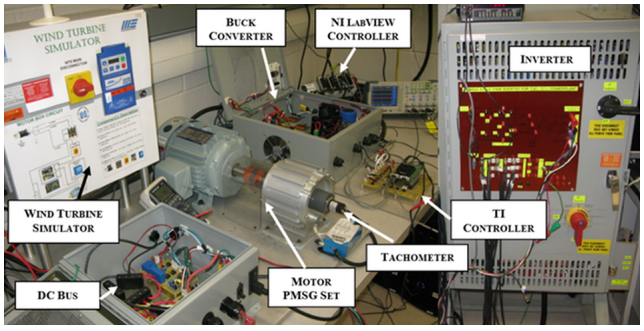

FIGURE 9. Experimental test facility.

An induction motor is used to drive the PMSG to emulate the wind turbine as the wind turbine simulator (WTS) [24]. A buck converter and an inverter have also been designed and fabricated to support this experiment. The grid is emulated by a commercial 1.5 kVA programmable three phase AC power source (model 310 HE, Pacific Power Source Corporation). The Texas Instruments (TI) controller and National Instruments (NI) LabVIEW controller are used to control the buck converter and WTS, respectively. The inverter control is implemented in dSPACE, and the data is collected through dSPACE control desk at a sampling interval of 290μs. The experiments are carried out under similar conditions as in the simulation *Section D Case Study IV*.

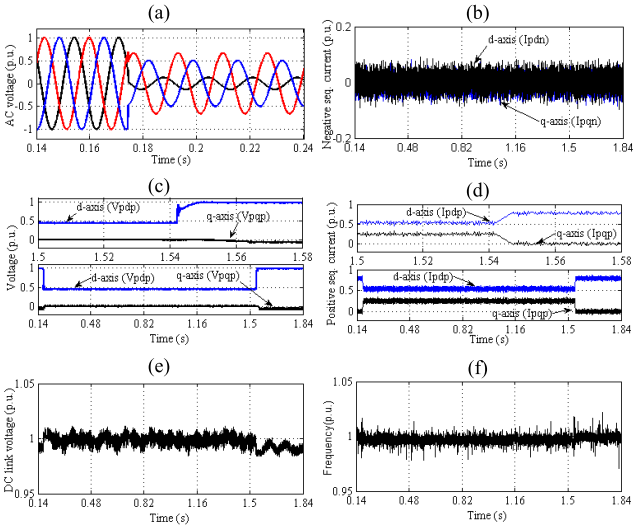

FIGURE 10. Behaviors of the system subject to an asymmetrical voltage sag with the SMC based control strategy (zoomed version at upper display for c and d): (a) AC voltage at the PCC; (b) Inverter negative sequence *d*- *q* axis currents; (c) Inverter positive sequence *d*- *q* axis voltages; (d) Inverter positive sequence *d*- *q* axis currents; (e) DC link voltage; and (f) Extracted per unit system frequency –omega (rad/s).

The experimental results are presented in Fig. 10. It is interesting to note the resemblance of the results to those in Fig. 8 based on simulations, except that the experiment results contain more noise. Both results have convincingly shown that the SMC based control strategy can eliminate oscillations and negative sequence components in the current injected to the grid and at the DLV. Furthermore, the inverter current can be maintained within the safe operating limit.

In summary, one can conclude that proposed control strategy based SMC can effectively deal with asymmetrical voltage sags at the PCC to ensure that the wind turbine system remains connected to the grid to supply the needed reactive power to support the grid voltage under unbalanced conditions.

VI. CONCLUSION

A VCCF of negative sequence voltage using sliding mode control strategy has been developed for a wind-turbine-driven PMSG system. The control objectives are to eliminate impacts of asymmetrical voltage sags at the PCC and to suppress the effects of disturbances. The investigation has concluded that sliding model control is more robust than conventional *PI* controller to achieve the above control

objectives. With the newly developed control scheme, the wind turbine system can remain connected to the grid during asymmetrical voltage sags and to provide adequate active and reactive power support. By doing so, the grid voltage at the PCC can be maintained. Four case studies have been carried out by simulations, and the performance of the control system has also been validated experimentally on a physical component based test facility. The experimental results have shown that the SMC control strategy can regulate the negative sequence current to zero, balance the power flow, and ensure the peak current within the safe operating limit.

APPENDIX

See Table 1.

TABLE 1. Parameters of wind system and the grid.

Grid voltage/frequency	170 [V]/60 [Hz]
Switching frequency	10 [kHz]
Rated power	1.0[kW]
DC link voltage	36 [V]
Rated rotational speed	900 [rpm]
Stator reactance	3.067 [Ohm]
Stator resistance	1.03 [Ohm]
Flux Linkage	0.1976 [Wb]
Number of poles	8
Air density	1.225 [kg/m^3]
Blade radius	1.2 [m]
Optimal power coefficient	0.43
Optimal tip speed ratio	6.28

REFERENCES

[1] O. Ozgener, "A small wind turbine system (SWTS) application and its performance analysis," *Energy Convers. Manag.*, vol. 47, pp. 1326–1337, Jul. 2006.

[2] S. M. Muyeen, R. Takahashi, T. Murata, and J. Tamura, "A variable speed wind turbine control strategy to meet wind farm grid code requirements," *IEEE Trans. Power Syst.*, vol. 25, no. 1, pp. 331–340, Feb. 2010.

[3] M. Martinez, A. Susperregui, G. Tapia, and L. Xu, "Sliding-mode control of a wind turbine-driven double-fed induction generator under non-ideal grid voltages," *IET Renew. Power Generat.*, vol. 7, no. 4, pp. 370–379, Jul. 2013.

[4] F. Blaabjerg, Z. Chen, and S. B. Kjaer, "Power electronics as efficient interface in dispersed power generation systems," *IEEE Trans. Power Electron.*, vol. 19, no. 5, pp. 1184–1194, Sep. 2004.

[5] F. Blaabjerg, M. Liserre, and K. Ma, "Power electronics converters for wind turbine systems," *IEEE Trans. Ind. Appl.*, vol. 48, no. 2, pp. 708–719, Mar./Apr. 2012.

[6] P. Rodriguez, A. V. Timbus, R. Teodorescu, M. Liserre, and F. Blaabjerg, "Flexible active power control of distributed power generation systems during grid faults," *IEEE Trans. Ind. Electron.*, vol. 54, no. 5, pp. 2583–2592, Oct. 2007.

[7] M. Chinchilla, S. Arnaltes, and J. C. Burgos, "Control of permanent-magnet generators applied to variable-speed wind-energy systems connected to the grid," *IEEE Trans. Energy Convers.*, vol. 21, no. 1, pp. 130–135, Mar. 2006.

[8] H.-S. Song and K. Nam, "Dual current control scheme for PWM converter under unbalanced input voltage conditions," *IEEE Trans. Ind. Electron.*, vol. 46, no. 5, pp. 953–959, Oct. 1999.

[9] P. Rioual, H. Pouliquen, and J.-P. Louis, "Regulation of a PWM rectifier in the unbalanced network state using a generalized model," *IEEE Trans. Power Electron.*, vol. 11, no. 3, pp. 495–502, May 1996.

[10] D. M. Lee, T. G. Habetler, R. G. Harley, T. L. Keister, and J. R. Rostron, "A voltage sag supporter utilizing a PWM-switched autotransformer," *IEEE Trans. Power Electron.*, vol. 22, no. 2, pp. 626–635, Mar. 2007.

[11] J. Eloy-Garcia, S. Arnaltes, and J. L. Rodriguez-Amenedo, "Direct power control of voltage source inverters with unbalanced grid voltages," *IET Power Electron.*, vol. 1, no. 3, pp. 395–407, Sep. 2008.

[12] J. Hu, J. Zhu, and D. G. Dorrell, "Model-predictive direct power control of doubly-fed induction generators under unbalanced grid voltage conditions in wind energy applications," *IET Renew. Power Generat.*, vol. 8, no. 6, pp. 687–695, Aug. 2014.

[13] A. Timbus, M. Liserre, R. Teodorescu, P. Rodriguez, and F. Blaabjerg, "Evaluation of current controllers for distributed power generation systems," *IEEE Trans. Power Electron.*, vol. 24, no. 3, pp. 654–664, Mar. 2009.

[14] E. Mamarelis, G. Petrone, and G. Spagnuolo, "Design of a sliding-mode-controlled SEPIC for PV MPPT applications," *IEEE Trans. Ind. Electron.*, vol. 61, no. 7, pp. 3387–3398, Jul. 2014.

[15] J. Hu, L. Shang, Y. He, and Z. Q. Zhu, "Direct active and reactive power regulation of grid-connected DC/AC converters using sliding mode control approach," *IEEE Trans. Power Electron.*, vol. 26, no. 1, pp. 210–222, Jan. 2011.

[16] J. Matas, M. Castilla, J. M. Guerrero, L. G. D. Vicuna, and J. Miret, "Feedback linearization of direct-drive synchronous wind-turbines via a sliding mode approach," *IEEE Trans. Power Electron.*, vol. 23, no. 3, pp. 1093–1103, May 2008.

[17] L. Shang, D. Sun, and J. Hu, "Sliding-mode-based direct power control of grid-connected voltage-sourced inverters under unbalanced network conditions," *IET Power Electron.*, vol. 4, no. 5, pp. 570–579, May 2011.

[18] L. Shang and J. Hu, "Sliding-mode-based direct power control of grid-connected wind-turbine-driven doubly fed induction generators under unbalanced grid voltage conditions," *IEEE Trans. Energy Convers.*, vol. 27, no. 2, pp. 362–373, Jun. 2012.

[19] J. Y. Hung, W. Gao, and J. C. Hung, "Variable structure control: A survey," *IEEE Trans. Ind. Electron.*, vol. 40, no. 1, pp. 2–22, Feb. 1993.

[20] S.-C. Tan, Y.-M. Lai, and C.-K. Tse, *Sliding Mode Control of Switching Power Converters*. Boca Raton, FL, USA: CRC Press, 2012.

[21] S. R. Sanders, J. M. Noworolski, X. Z. Liu, and G. C. Verghese, "Generalized averaging method for power conversion circuits," *IEEE Trans. Power Electron.*, vol. 6, no. 2, pp. 251–259, Apr. 1991.

[22] A. Yazdani and R. Iravani, *Voltage-Sourced Converters in Power Systems : Modeling, Control, and Applications*. Hoboken, NJ, USA: Wiley,2010.

[23] A. Moharana and P. K. Dash, "Input-output linearization and robust sliding-mode controller for the VSC-HVDC transmission link," *IEEE Trans. Power Del.*, vol. 25, no. 3, pp. 1952–1961, Jul. 2010.

[24] D. Thakur and J. Jiang, "Design and construction of a wind turbine simulator for integration to a microgrid with renewable energy sources," *Electr. Power Compon. Syst.*, vol. 45, no. 9, pp. 949–963, May 2017.

DEVBRATTA THAKUR received the Ph.D. degree from the Department of Electrical and Computer Engineering, University of Western Ontario, London, ON, Canada, in 2015. He is currently with Canadian Solar Inc. His research interests include the integration, control, and performance enhancement of renewable energy, microgrids, and power electronic converters for power system applications, grid operation, and power system optimization in the context of smart grids.

JIN JIANG received the Ph.D. degree from the University of New Brunswick, Fredericton, NB, Canada, in 1989. Since 1991, he has been with the Department of Electrical and Computer Engineering, University of Western Ontario, London, ON, Canada, where he is currently a Distinguished University Professor and a Senior Industrial Research Chair. His research interests include fault-tolerant control of safety-critical systems, advanced control of electrical power plants and power systems, and energy management and control of microgrids involving renewable energy resources. He is a Fellow of the Canadian Academy of Engineering. He is also a Member of the International Electrotechnical Commission 45A.